

# Electronic, dynamical and superconducting properties of CaBeSi

C. Bersier,<sup>1,2</sup> A. Floris,<sup>1,2</sup> A. Sanna,<sup>1,2,3</sup> G. Profeta,<sup>4</sup> A. Continenza,<sup>4</sup> E. K. U. Gross,<sup>1,2</sup> and S. Massidda<sup>3</sup>

<sup>1</sup>*Institut für Theoretische Physik, Freie Universität Berlin, Arnimallee 14, D-14195 Berlin, Germany*

<sup>2</sup>*European Theoretical Spectroscopy Facility (ETSF)*

<sup>3</sup>*INFM SLACS, Sardinian Laboratory for Computational Materials Science and Dipartimento di Scienze Fisiche, Università degli Studi di Cagliari, S.P. Monserrato-Sestu km 0.700, I-09124 Monserrato (Cagliari), Italy*

<sup>4</sup>*CNISM - Dipartimento di Fisica, Università degli Studi dell'Aquila, Via Vetoio 10, I-67010 Coppito (L'Aquila) Italy*

(Dated: December 1, 2018)

We report first-principles calculations on the normal and superconducting state of  $\text{CaBe}_x\text{Si}_{2-x}$  ( $x = 1$ ), in the framework of density functional theory for superconductors (SCDFT).  $\text{CaBeSi}$  is isostructural and isoelectronic to  $\text{MgB}_2$  and this makes possible a direct comparison of the electronic and vibrational properties and the electron-phonon interaction of the two materials. Despite the many similarities with  $\text{MgB}_2$  (e.g.  $\sigma$  bands at the Fermi level and a larger Fermi surface nesting), according to our calculations  $\text{CaBeSi}$  has a very low critical temperature ( $T_c \approx 0.4$  K, consistent with the experiment).  $\text{CaBeSi}$  exhibits a complex gap structure, with three gaps at Fermi level: besides the two  $\sigma$  and  $\pi$  gaps, present also in  $\text{MgB}_2$ , the appearance of a third gap is related to the anisotropy of the Coulomb repulsion, acting in different way on the bonding and antibonding electronic  $\pi$  states.

PACS numbers: 74.25.Jb, 74.25.Kc, 74.70.Ad

## I. INTRODUCTION

The complexity and the fragility of the effective pairing interaction – result of a fine interplay of opposite contributions – and its non-trivial dependence on chemical properties make the search of new superconducting materials a very difficult task, even within the class of phonon mediated superconductors. As a result, research often goes along the lines of searching in the “neighborhood” of known superconductors. This has been the case of  $\text{MgB}_2$  that owes its superconducting (SC) properties<sup>1,2,3</sup> essentially to the presence of holes in the  $sp^2$   $\sigma$  B-B covalent bonds, strongly coupled with the  $E_{2g}$  stretching mode. During the last years,  $\text{MgB}_2$  boosted experimental and theoretical research in the class of diborides, layered, graphite-like materials, all sharing some hopefully relevant features with the “parent compound”. Although this effort did not succeed in finding superconductors with better (or at least equivalent) properties than  $\text{MgB}_2$ , it brought to the experimental discovery of some new superconductors like graphite intercalated compounds,<sup>4,5</sup> boron doped diamond,<sup>6</sup> and to some theoretical proposals.<sup>7,8</sup>

Among  $\text{MgB}_2$ -like materials, one interesting case is represented by  $\text{CaSi}_2$ , which at ambient pressure has a rhombohedral structure and changes to a trigonal phase between  $\approx 7$  and 9.5 GPa. At  $P > 16$  GPa,  $\text{CaSi}_2$  has the  $AlB_2$  structure and SC critical temperatures ( $T_c$ ) up to 14 K. The stability of the  $AlB_2$  phase at ambient pressure is achieved through hole doping. The stabilization process has been related<sup>9</sup> to the filling of the  $\pi$  antibonding bands ( $\pi_a$ ). Let us consider a material  $\text{CaX}_x\text{Si}_{2-x}$  (X having a lower valence than Si): increasing  $x$  from zero introduces holes in the  $\pi_a$  bands, with a change in the X-Si bond that from an  $sp^3$ -like character acquires a progressive  $sp^2$  character, stabilizing the  $AlB_2$  structure.<sup>9</sup>

Thus, hole-doped  $\text{CaSi}_2$  could represent (with some differences) a good candidate for an  $\text{MgB}_2$ -like material, although its stabilization at high pressure poses some problems. Nevertheless, experimentally, the  $AlB_2$  phase was observed at ambient pressure by doping  $\text{CaSi}_2$  with Al<sup>10,11</sup> or, in a much less studied case, with Be.<sup>12,13</sup> Recently,  $\text{CaBe}_x\text{Si}_{2-x}$  was investigated in the doping range  $0.5 \leq x \leq 1$ <sup>13</sup> and was observed to have the  $AlB_2$  structure at  $x = 0.75$ <sup>12,13</sup> and, against the expectations, not to be a superconductor down to 4.2 K.<sup>13</sup>

The goal of this paper is to clarify why this happens despite the presence of  $\sigma$  holes, as in  $\text{MgB}_2$ , and an even more pronounced nesting. We investigate the normal and SC phase of  $\text{CaBe}_x\text{Si}_{2-x}$  at  $x = 1$  ( $\text{CaBeSi}$  in the following),<sup>14</sup> in the  $AlB_2$  phase, with Be and Si atoms alternating within the honeycomb layers with an  $AA$  stacking.

The paper is organized as follows: In Secs. II and III we sketch our computational framework and describe the computational details of our calculations. In Sec. IV we illustrate the normal state properties and the e-phon coupling of  $\text{CaBeSi}$ . The superconducting properties are discussed in Sec. V. Finally, in Sec. VI, we summarize our results.

## II. DENSITY FUNCTIONAL THEORY FOR SUPERCONDUCTORS (SCDFT)

The superconducting properties are studied within the density functional theory for superconductivity (SCDFT),<sup>15,16</sup> a completely parameter free approach which allows to predict the SC gap and  $T_c$  values of real materials.<sup>15,16</sup> As the SCDFT method was discussed in full detail in previous papers,<sup>15,16</sup> here we only sketch the main points concerning the theory, whose central result

is the generalized, self-consistent, gap equation:

$$\Delta_{n\mathbf{k}} = -\mathcal{Z}_{n\mathbf{k}} \Delta_{n\mathbf{k}} - \frac{1}{2} \sum_{n'\mathbf{k}'} \mathcal{K}_{n\mathbf{k},n'\mathbf{k}'} \frac{\tanh\left(\frac{\beta}{2} E_{n'\mathbf{k}'}\right)}{E_{n'\mathbf{k}'}} \Delta_{n'\mathbf{k}'}, \quad (1)$$

where  $n$  and  $\mathbf{k}$  are respectively the electronic band index and the Bloch wave vector;  $\Delta_{n\mathbf{k}}$  is the SC gap function;  $\beta$  is the inverse temperature;  $E_{n\mathbf{k}} = \sqrt{(\varepsilon_{n\mathbf{k}} - \mu)^2 + |\Delta_{n\mathbf{k}}|^2}$  are the SC quasiparticle energies, defined in terms of the gap function, the Kohn-Sham eigenenergies  $\varepsilon_{n\mathbf{k}}$  of the normal state and the chemical potential  $\mu$ . The *universal* kernel  $\mathcal{K}_{n\mathbf{k},n'\mathbf{k}'}$  appearing in Eq. (1) consists of two contributions  $\mathcal{K} = \mathcal{K}^{\text{e-ph}} + \mathcal{K}^{\text{e-e}}$ , representing the effects of the e-ph and the e-e interactions respectively.  $\mathcal{K}^{\text{e-ph}}$  is temperature dependent and involves the e-ph coupling matrix elements  $|g_{\mathbf{k},\mathbf{k}',\nu}^{nn'}|^2$  and the phonon spectrum  $\omega_{\mathbf{q}\nu}$ , while  $\mathcal{K}^{\text{e-e}}$  contains the matrix elements of the screened Coulomb repulsion. Finally, the *universal* diagonal (and temperature dependent) term  $\mathcal{Z}_{n\mathbf{k}}$  plays a similar role as the renormalization term in the Eliashberg equations. We emphasize that Eq. (1) is not a mean-field equation (as in BCS theory), since it contains correlation effects via the SC exchange-correlation (xc) functional entering  $\mathcal{K}$  and  $\mathcal{Z}$ . Furthermore, it has the form of a static equation – i.e., it does not depend *explicitly* on the frequency – and therefore has a simpler structure (and computationally more manageable) than the Eliashberg equations. However, this certainly does not imply that retardation effects are absent from the theory. Once again, retardation effects enter through the xc functional, as explained in Refs. 15,16 .

An important feature of the SCDFT approach is the capability to include the  $n\mathbf{k}$ -resolved Coulomb repulsion  $V^{\text{e-e}}$  *ab-initio*, without any adjustable parameter. The Coulomb interaction was screened with a static dielectric matrix, within the Random Phase Approximation (RPA)<sup>17</sup>(see below).

### III. COMPUTATIONAL DETAILS

The electronic band structure  $\varepsilon_{n\mathbf{k}}$ , the phonon spectrum  $\omega_{\mathbf{q}\nu}$ , and the electron-phonon (e-ph) and Coulomb matrix elements (ME) with respect to the Bloch functions necessary to solve the SC gap (Eq. 1), were obtained within the planewave-pseudopotential method.<sup>18</sup> We used Troullier-Martins,<sup>19</sup> norm-conserving pseudopotentials,<sup>20</sup> with 2s, 3s-3p and 3s-3p-4s for Be, Si and Ca, respectively, in the GGA-PBE<sup>21</sup> approximation for the xc functional. The electronic self-consistent cycle was performed with a 60 Ry energy cut-off, a 18<sup>3</sup> Monkhorst-Pack  $\mathbf{k}$ -point mesh.

The optimized lattice parameters (at  $x = 1$  Be doping) are  $a = 3.895$  Å and  $c/a = 1.112$ , whereas the experimental values (at  $x = 0.75$ ) are  $a = 3.94$  Å and  $c/a = 1.112$ .<sup>12,13</sup> Our obtained, slightly smaller GGA-PBE  $a$  constant is justified by the larger amount of Be

	$a$	$c$	Si-Si	Si-Be	B-B
CaBeSi	3.895	4.331	3.895	2.249	-
MgB <sub>2</sub> <sup>a</sup>	3.083	3.52	-	-	1.780

<sup>a</sup>Experimental constants

TABLE I: Structural parameters (in Å) of CaBeSi and MgB<sub>2</sub>.

(with smaller covalent radius than Si) present in the calculated system.

Phonons and e-ph ME were calculated via density functional perturbation theory.<sup>23</sup> The phonons were computed on the irreducible set of a regular mesh of 8<sup>3</sup>  $\mathbf{q}$ -points, and a 16<sup>3</sup> Monkhorst-Pack  $\mathbf{k}$ -points for electronic integration, with a smearing parameter of 0.35 eV. These parameters were sufficient to achieve convergence within 0.5 meV in the frequency of the  $E_{2g}(\Gamma)$  mode. Our calculated  $\omega_{E_{2g}}(\Gamma) = 59.0$  meV compares well with the value  $\omega_{E_{2g}}(\Gamma) = 57.1$  meV obtained by frozen phonon calculations in Ref. 9, computed at the slightly larger  $a = 3.914$  Å. The e-ph ME were calculated on the same  $\mathbf{q}$ -points grid as the phonons, and on a denser grid of 24<sup>3</sup>  $\mathbf{k}$ -points, while the RPA screened Coulomb ME were calculated<sup>17</sup> on a mesh of 9<sup>3</sup>  $\times$  9<sup>3</sup>  $\mathbf{k}$  and  $\mathbf{k}'$ -points. The SC gap function is extremely peaked around the Fermi surface (within the characteristic phonon energy), whereas at higher energies it is rather smooth (and it changes sign, due to the e-e interaction). This implies that a converged solution of Eq. (1) needs a denser  $\mathbf{k}$ -points sampling around  $E_F$ , while a coarser one is sufficient elsewhere. This highly non uniform mesh of the Brillouin zone is realized with  $8 \times 10^3$  and 500 independent  $\mathbf{k}$ -points for bands crossing and not crossing the Fermi level respectively. Finally, 15-20 self consistent iterations were sufficient to achieve a complete convergence of the gap.

## IV. NORMAL STATE PROPERTIES

### A. Electronic structure and Fermi surface

Fig. 1 shows the CaBeSi and MgB<sub>2</sub> band structure. A general similarity is found: in both materials the  $\sigma$ ,  $\pi$ -bonding ( $\pi_b$ ) and  $\pi$ -antibonding ( $\pi_a$ ) bands cross the Fermi level ( $E_F$ ). As pointed out in Ref. 9, and similarly to CaAlSi,<sup>24</sup> the reduced symmetry (space group P6m2) with respect to MgB<sub>2</sub> (P6/mmm), related to the partially ionic nature of the B-Si bond, implies the splittings of the  $\sigma$  and the  $\pi_b$ - $\pi_a$  bands at the K and H points of the Brillouin zone (BZ). In CaBeSi the  $\pi_b$  bands are almost fully occupied, leaving only small holes pockets at K which give rise to the little  $\pi$  spheres of the Fermi surface (FS) (see Fig. 2). These replace the  $\pi$  tubular structure present in MgB<sub>2</sub>. The  $\pi_a$  bands are only partially occupied, allowing the stabilization of the Si-Be  $sp^2$  network against a  $sp^3$ -like distortion. In fact, the latter

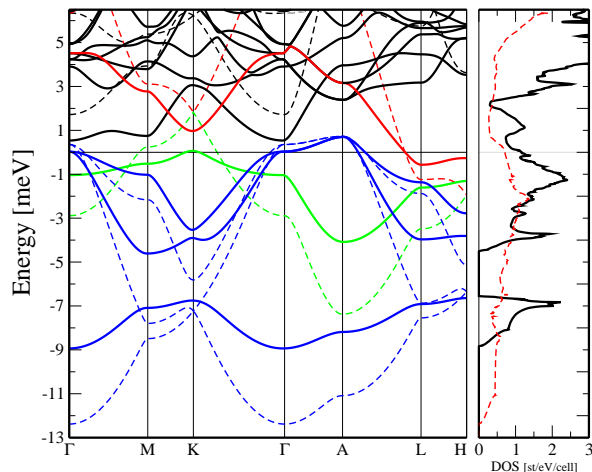


FIG. 1: (color online) Band structure and DOS of CaBeSi (full lines) and MgB<sub>2</sub> (dashed lines). Colors refer to different characters:  $\sigma$  (blue),  $\pi$  bonding (green),  $\pi$  antibonding (red).

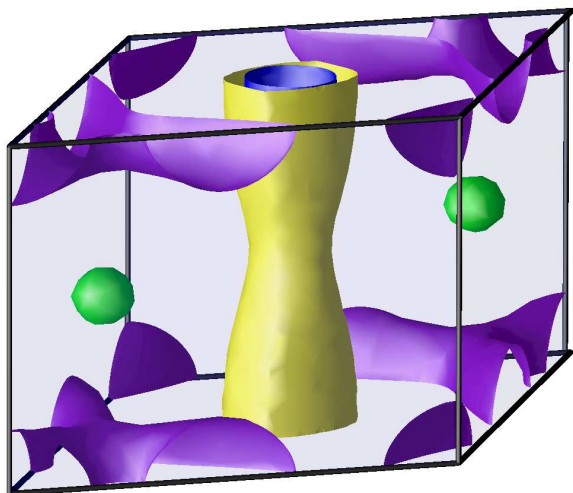


FIG. 2: (color online) CaBeSi Fermi surface. The colors identify the three gaps at  $E_F$ : the largest  $\sigma$  (yellow and blue cylindrical-like sheets); the intermediate  $\pi$  bonding (green spheres); the lowest  $\pi$  antibonding (violet).

takes place in the presence of a larger amount of Si, *i.e.* with a larger filling of the  $\pi_a$  bands.<sup>9</sup>

Due to the different electronegativity of Si and Be, we expect a change in the charge distribution related to their bond, in comparison with the B-B bond in MgB<sub>2</sub>. In Fig. 3 (upper panel) we plot the  $\pi_b$  and  $\pi_a$  charge at the BZ H point. We see that the  $\pi_b$  ( $\pi_a$ ) charge is clearly associated to the Si (Be) atom. Having in mind the different occupation of the  $\pi_b$  and  $\pi_a$  bands, we conclude that there is a charge disproportion in favor of Si.

Another important chemical difference between MgB<sub>2</sub> and CaBeSi is the presence of Ca- $d$  states at  $\sim 5$  eV above  $E_F$  that strongly interact with  $\pi$  and  $\sigma$  bands, in different

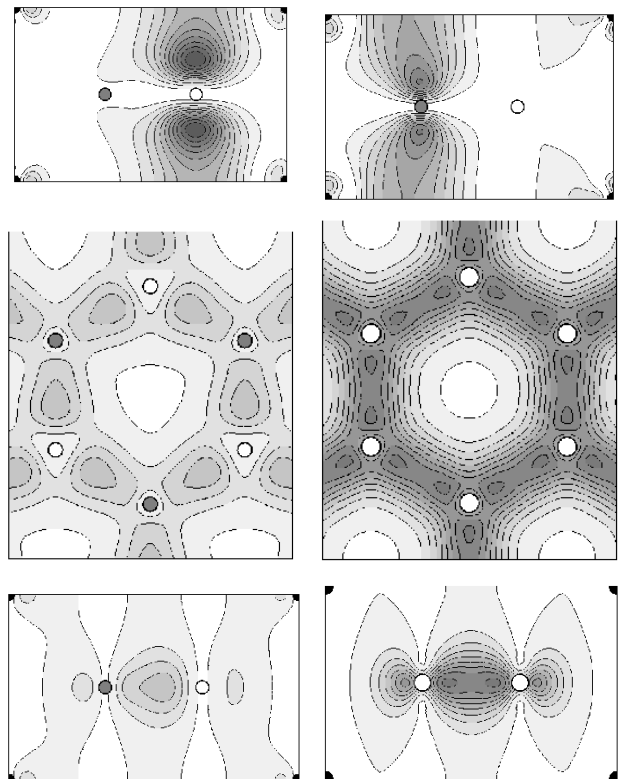


FIG. 3: CaBeSi and MgB<sub>2</sub> charge. Upper panel: CaBeSi  $\pi$  bonding (left) and  $\pi$  antibonding (right) charge at the H point; empty (full) circle refers to Si (Be). Middle and lower panels: CaBeSi (left) and MgB<sub>2</sub> (right)  $\sigma$  charge at the  $\Gamma$  point; in the middle (lower) panel, the  $z$  direction is perpendicular (parallel) to the page.

ways along the zone. This contributes to the reduced in plane  $\pi$  bandwidth ( $\approx 1.1$  eV and  $\approx 2.8$  eV along  $\Gamma$ MK and ALH) in CaBeSi with respect to MgB<sub>2</sub> ( $\approx 5.5$  eV). In fact, while at the  $\Gamma$  point there is no interaction between  $\pi$  states and the cation  $d$  orbitals, the interaction is possible in the high symmetry points A, M and K, therefore suppressing the large dispersion of these states observed in MgB<sub>2</sub>. A further reason for the reduced  $\pi$  bandwidth in CaBeSi is a lower chemical pressure effect due to its larger unit cell in comparison to MgB<sub>2</sub>.

Looking at the  $\sigma$  charge in the two materials (Fig. 3, middle and lower panels), we notice a stronger localization in MgB<sub>2</sub> along the B-B direction, whereas in CaBeSi the  $\sigma$  charge has a clear ionic component and is more delocalized both in the in-plane and out-of-plane directions. This makes the Si-Be bond much weaker than the B-B one affecting the strength of the e-ph coupling.

As far as the  $\sigma$  bandwidth is concerned, the larger Si-Be distance (see Table I) and a lower Si-Be interaction (compared to B-B) explain the reduced in plane  $\sigma$ -band dispersion (for the lower  $\sigma \approx 5$  eV and  $\approx 8$  eV in CaBeSi and MgB<sub>2</sub>, respectively). On the other hand, the larger out of plane dispersion of  $\sigma$  bands in CaBeSi ( $\approx 1$  eV)

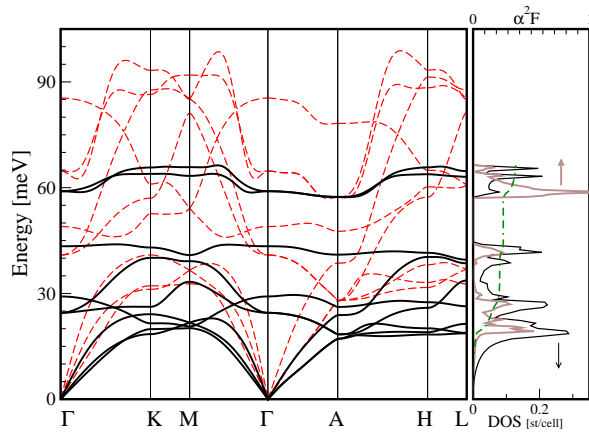


FIG. 4: (color online) Left panel: phonon structure of CaBeSi (full lines) and MgB<sub>2</sub> (dashed lines). Right panel: CaBeSi phonon DOS (thin black line), Eliashberg function (thick brown line) and integration curve  $2 \int_0^\omega \alpha^2 F(\omega') / \omega' d\omega'$  (dot-dashed green line), whose final value is the total e-ph coupling  $\lambda$ .

versus MgB<sub>2</sub> ( $\approx 0.5$  eV) is only partially justified with the larger  $z$ -extension of the CaBeSi  $\sigma$  charge (compensated by the  $\approx 25\%$  larger interlayer distance), and is mainly related to the  $\sigma - \text{Ca}-d_{x^2-y^2}$  interaction allowed at the  $\Gamma$  point but not at A (see Fig. 1). Difference in band dispersion gives rise to much of the warping of the corresponding Fermi surface.

## B. Phonons and electron-phonon coupling

The previous discussion shows that, despite the general similarities, CaBeSi and MgB<sub>2</sub> have rather different chemical and electronic properties. As expected, they determine both the dynamical properties and the electron-phonon coupling. In fact, CaBeSi frequencies are lower (see Fig. 4) in comparison with MgB<sub>2</sub>, mainly due to the larger mass of Ca and Si versus Mg and B.

The  $E_{2g}$  mode is fairly flat along the in plane BZ symmetry lines and it shows only a very weak renormalization along  $\text{M}\Gamma$  and  $\text{A}\text{H}$  lines (four times smaller than in MgB<sub>2</sub>)<sup>3,25,26</sup> due to the very small  $E_{2g}$  electron-phonon matrix elements. In turn, this is related to the delocalized and ionic nature of the  $\sigma$  bonds in CaBeSi (see Fig. 3). In fact, the connection between strongly covalent bonds and strong e-ph coupling seems to be a general feature.<sup>1,27,28,29</sup>

The  $B_{1g}$  mode lower than the  $E_{2g}$  everywhere in the BZ, without exhibiting the features found in CaAlSi, where it is very soft, due to a strong interband coupling between the interlayer and  $\pi_a$  states.<sup>24</sup>

The strongly reduced e-ph renormalization of the CaBeSi  $E_{2g}$  mode is not related to poor FS nesting features in this material, but only to the small value of the e-ph ME themselves. In fact, we have calculated the

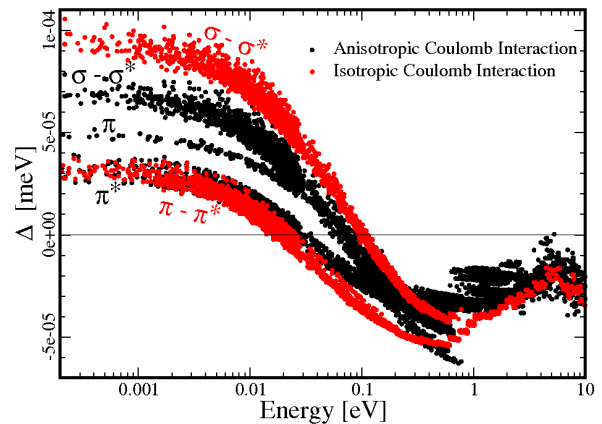


FIG. 5: (color online) CaBeSi superconducting gap as a function of the energy distance from the Fermi level.

$\sigma$  nesting function  $\eta_q^\sigma = \frac{1}{N_\sigma(0)} \sum_{\mathbf{k} \in \sigma} \delta(\epsilon_{\mathbf{k}}) \delta(\epsilon_{\mathbf{k}+\mathbf{q}})$  (where  $\mathbf{k} + \mathbf{q} \in \sigma$  and  $N_\sigma(0)$  is the  $\sigma$  DOS at  $E_F$ ), obtaining *larger* values for CaBeSi than for MgB<sub>2</sub> (roughly a factor of 2).

The calculated total e-ph is  $\lambda = 0.38$ , which makes CaBeSi a weak coupling superconductor, comparable to Al or Mo, with a  $T_c = 0.4$  K. The two-band resolved values (see Eq. 3) are  $\lambda_{\sigma\sigma} = 0.29$ ;  $\lambda_{\sigma\pi} = 0.21$ ;  $\lambda_{\pi\sigma} = 0.15$ ;  $\lambda_{\pi\pi} = 0.12$  whereas the MgB<sub>2</sub> values are<sup>30</sup>  $\lambda_{\sigma\sigma} = 0.83$ ;  $\lambda_{\sigma\pi} = 0.22$ ;  $\lambda_{\pi\sigma} = 0.16$ ;  $\lambda_{\pi\pi} = 0.28$ . The comparison further shows the dramatic reduction of the  $\sigma$ - $\sigma$  coupling in CaBeSi.

Although weaker than in MgB<sub>2</sub>, the contribution from the  $E_{2g}$  mode is important also in the CaBeSi Eliashberg function (Fig. 4), where we see a peak at  $\sim 60$  meV which strongly enhances a corresponding structure in the phonon density of states. This peak gives roughly one fourth of the total e-ph coupling, while the main contribution to the coupling comes from low frequency modes.

We note that charge localization not only enhances the e-ph interaction, but also the Coulomb ME,<sup>31</sup> which are lower in CaBeSi than in MgB<sub>2</sub>. However, this reduction is not so dramatic as for the e-ph ME. This is due to the different structure of the ME of the two interactions (see discussion below).

## V. SUPERCONDUCTING STATE

The solution of the self-consistent gap equation (Eq. (1)) including the anisotropic e-ph ME  $|g_{\mathbf{k},\mathbf{k}'}^{nn'}|^2$  and, the  $n\mathbf{k}$ -resolved RPA Coulomb matrix elements  $V_{n\mathbf{k},n'\mathbf{k}'}^{e-e}$ , reveals an unexpected complex structure with clearly separated *three* gaps at  $E_F$  (Fig. 5). The calculated critical temperature is very low ( $T_c = 0.4$ ), lower than the upper limit (4.2 K) set by the experimental results.<sup>13</sup> Unlike in MgB<sub>2</sub>, in which superconductivity is interpreted within a two-band model,<sup>2,32,33,34</sup> in CaBeSi there is a further  $\pi_b$ - $\pi_a$  gap splitting. As in MgB<sub>2</sub>, the largest gap is related to the  $\sigma$  FS sheets (cylindrical-like structures in Fig. 2), the intermediate one to  $\pi_b$  sheets (small hole spheres) and the lowest to  $\pi_a$  sheets. The additional  $\pi_b$ - $\pi_a$  gap splitting is a peculiar feature of CaBeSi not present in MgB<sub>2</sub> in which the two  $\sigma$  and the two  $\pi$  gaps merge together.

In order to understand the origin of this splitting we perform some additional computational experiments, solving the gap equation (i) completely neglecting the Coulomb interaction, (ii) including only the averaged Coulomb term

$$V_{av}^{e-e}(\epsilon, \epsilon') = \frac{1}{N(\epsilon)N(\epsilon')} \sum_{n\mathbf{k}, n'\mathbf{k}'} V_{n\mathbf{k}, n'\mathbf{k}'}^{e-e} \times \delta(\epsilon_{n\mathbf{k}} - \epsilon) \delta(\epsilon_{n'\mathbf{k}'} - \epsilon'). \quad (2)$$

and (iii) with isotropically averaged Coulomb and phononic interactions, corresponding to the dirty limit.

In both (i) and (ii) cases, the three gap structure is destroyed, bringing back to a two-band, MgB<sub>2</sub>-like gap structure. In case (iii), instead, superconductivity is completely lost. As a result, we predict superconductivity in CaBeSi *only* if the anisotropic structure of the interactions is included. In the real system, very likely, disorder on the Si-Be sublattice can produce interband  $\pi$ - $\sigma$  impurity scattering, therefore reducing  $T_c$  further.

In the following we will analyse the three gap structure, with particular emphasis in understanding the  $\pi_b$ - $\pi_a$  splitting observed. To this purpose, we perform a four-band model analysis, splitting the Fermi surface in: internal  $\sigma$  band ( $\sigma_1$ ), external  $\sigma$  band ( $\sigma_2$ ),  $\pi_b$  and  $\pi_a$  bands.

We have calculated (see Table II *a* and *b*) the corresponding density of states  $N_n$  and the BCS-like e-ph couplings,  $\lambda_{nn'}$  and  $V_{nn'}^{e-ph}$ , where:

$$\lambda_{nn'} = V_{nn'}^{e-ph} N_{n'} \quad (3)$$

and

$$V_{nn'}^{e-ph} = \frac{2}{N_n N_{n'}} \sum_{\mathbf{k} \in n, \mathbf{k}' \in n'} \sum_{\nu} \frac{|g_{\mathbf{k}, \mathbf{k}', \nu}^{nn'}|^2}{\omega_{\mathbf{k}' - \mathbf{k}, \nu}} \times \delta(\epsilon_{n\mathbf{k}} - E_F) \delta(\epsilon_{n'\mathbf{k}'} - E_F). \quad (4)$$

First, we notice that the  $\sigma$  submatrix  $V_{\sigma\sigma}^{e-ph}$  is very homogeneous. Second, the  $\sigma$ - $\pi$  scattering gives the same contribution to both  $\sigma$  gaps, which are then identical. Superconductivity in the  $\pi$  states is more complicated, essentially because, unlike  $\sigma$  bands,  $\pi_a$  and  $\pi_b$  bands originate from different sublattices. As a consequence, the  $\pi$  submatrix is not homogeneous. Moreover, the  $\pi$ - $\sigma$  interaction is of the same size of the  $\pi$ - $\pi$  one, and  $\pi_a$  and  $\pi_b$  have different density of states, being  $N_{\pi_a} \simeq 6 \cdot N_{\pi_b}$ . In order to understand the qualitative structure of the SCDF T results, we considered a BCS-type approximation of the 4-band Eliashberg equations.<sup>35</sup> This model calculation confirms that the inclusion of the average Coulomb interaction (Eq. 2), does not produce  $\pi_b$ - $\pi_a$  gap splitting. In fact, the splitting is recovered *only* considering the (band) anisotropic  $V_{nn'}^{e-e}$  Coulomb ME, reported in Table IIc. These are, as for the el-ph coupling, roughly homogeneous in the  $\sigma$  submatrix and therefore not able to split the  $\sigma$  gap, but in the  $V_{\pi\pi}^{e-e}$  submatrix, the intraband interaction is  $\approx 2.7$  times larger than the interband interaction (that couples states in different sublattices). The huge difference between  $V_{\pi_b\pi_a}^{e-e}$  and  $V_{\pi_a\pi_a}^{e-e}$  and the low  $N_{\pi_b}$  (that makes the  $\mu_{\pi_b\pi_b}$  and  $\mu_{\pi_a\pi_b}$  negligible), lead to a much stronger suppression of  $\Delta_{\pi_a}$  relative to  $\Delta_{\pi_b}$ , eventually bringing to the three gap structure.

<i>a</i>	dos	$\sigma_1$	$\sigma_2$	$\pi_b$	$\pi_a$
	$N$	0.12	0.38	0.1	0.58

<i>b</i>	e-ph	$\sigma_1$	$\sigma_2$	$\pi_b$	$\pi_a$
	$\sigma_1$	<b>0.07</b>	<b>0.23</b>	<b>0.03</b>	<b>0.20</b>
		(0.62)	(0.61)	(0.28)	(0.34)
	$\sigma_2$	<b>0.07</b>	<b>0.22</b>	<b>0.02</b>	<b>0.19</b>
		(0.61)	(0.57)	(0.23)	(0.32)
	$\pi_b$	<b>0.03</b>	<b>0.09</b>	<b>0.03</b>	<b>0.16</b>
		(0.28)	(0.23)	(0.35)	(0.28)
	$\pi_a$	<b>0.04</b>	<b>0.12</b>	<b>0.03</b>	<b>0.07</b>
		(0.34)	(0.32)	(0.28)	(0.12)

<i>c</i>	el-el	$\sigma_1$	$\sigma_2$	$\pi_b$	$\pi_a$
	$\sigma_1$	<b>0.11</b>	<b>0.27</b>	<b>0.03</b>	<b>0.15</b>
		(0.91)	(0.71)	(0.30)	(0.26)
	$\sigma_2$	<b>0.08</b>	<b>0.32</b>	<b>0.03</b>	<b>0.13</b>
		(0.71)	(0.84)	(0.29)	(0.23)
	$\pi_b$	<b>0.04</b>	<b>0.11</b>	<b>0.09</b>	<b>0.20</b>
		(0.30)	(0.29)	(0.94)	(0.35)
	$\pi_a$	<b>0.03</b>	<b>0.09</b>	<b>0.03</b>	<b>0.51</b>
		(0.26)	(0.23)	(0.35)	(0.86)

TABLE II: Table *a*: Band resolved density of states [st/(cell-eV)]. Table *b*: Band resolved e-ph couplings  $\lambda_{nn'}$  (in bold) and BCS effective potentials  $V_{nn'}^{e-ph} = \lambda_{nn'}/N'_n$  (in parenthesis [eV]). Table *c*: Band resolved el-el interactions at the Fermi energy  $\mu_{nn'}$  (in bold), and el-el matrix elements  $V_{nn'}^{e-e}$  at the Fermi energy (in parenthesis [eV]).

## VI. SUMMARY AND CONCLUSIONS

We have calculated the normal and superconducting state properties of CaBe<sub>x</sub>Si<sub>2-x</sub> ( $x = 1$ ) in the  $AlB_2$  phase, within the density functional theory for superconductors (SCDFT). The chosen doping level is not far from the experimental doping ( $x = 0.75$ ) where this phase is found stable and homogeneous. CaBeSi is isostructural and isoelectronic to MgB<sub>2</sub> and the electronic, vibrational properties and electron-phonon interaction of the two materials are compared directly: While the band structures present strong similarities, with both  $\sigma$  and  $\pi$  bands crossing the Fermi level, the phonon structure and the e-ph interaction differ substantially. In particular, the less localized  $\sigma$  charge of CaBeSi brings to a dramatic reduction in the  $E_{2g}$  electron-phonon coupling, with a consequent reduction of the phonon renormalization seen in MgB<sub>2</sub>. This fact makes CaBeSi a weak coupling superconductor with e-ph  $\lambda = 0.38$  and  $T_c = 0.4$  K, in spite of a nesting at the Fermi surface twice as big as in MgB<sub>2</sub>. Interestingly, CaBeSi exhibits three superconducting gaps at the Fermi level. While, as in MgB<sub>2</sub>, the  $\sigma$ - $\pi$  gap splitting is related to the different e-ph

coupling in these bands, the further  $\pi_b$ - $\pi_a$  splitting is a pure effect of the complex structure of the anisotropic Coulomb repulsion, acting in different way on the  $\pi_b$  and  $\pi_a$  states.

## VII. ACKNOWLEDGMENTS

The Authors thank A. Marini for technical support and for making the SELF code available. This work was supported by the Italian Ministry of Education, through a 2004

PRIN project, by the Istituto Nazionale di Fisica della Materia (INFN-CNR) through a supercomputing grant at Cineca (Bologna, Italy), by MIUR under project PONCyberSar, and by the Deutsche Forschungsgemeinschaft, by the EXCITING Network and by the NANOQUANTA Network of Excellence. A.F. acknowledges CNISM for financial support during his visit in University of L'Aquila. A.S. acknowledges the *Regione Autonoma della Sardegna* for providing the Master and Back fellowship. C.B. acknowledges for the financial support of the Swiss National Science Foundation.

- <sup>1</sup> J. M. An and W.E. Pickett, Phys. Rev. Lett. **86**, 4366 (2001).
- <sup>2</sup> A. Y. Liu, I. I. Mazin, J. Kortus, Phys. Rev. Lett. **87**, 087005 (2001).
- <sup>3</sup> Y. Kong, O. V. Dolgov, O. Jepsen, O. K. Andersen, Phys. Rev. B **64**, 020501 (2001).
- <sup>4</sup> T. E. Weller, M. Ellerby, S. S. Saxena, R. P. Smith, and N. T. Skipper, Nature Phys. **1**, 39 (2005).
- <sup>5</sup> N. Emery, C. Hérodol, M. d'Astuto, V. Garcia, Ch. Bellin, J. F. Maréché, P. Lagrange, and G. Loupiau, Phys. Rev. Lett. **95**, 087003 (2005).
- <sup>6</sup> E. A. Ekimov, V. A. Sidorov, E. D. Bauer, N. N. Mel'nik, N. J. Curro, J. D. Thompson, S. M. Stishov, Nature **428**, 542 (2004)
- <sup>7</sup> H. Rosner, A. Kitaigorodsky and W.E. Pickett, Phys. Rev. Lett. **88**, 127001 (2002).
- <sup>8</sup> F. J. Ribeiro and M. L. Cohen, Phys. Rev. B **69**, 212507 (2004).
- <sup>9</sup> G. Satta, G. Profeta, F. Bernardini, A. Continenza, and S. Massidda, PRB **64**, 104507 (2001).
- <sup>10</sup> M. Imai, K. Nishida, T. Kimura and H. Abe, Appl. Phys. Lett. **80**, 1019 (2001).
- <sup>11</sup> B. Lorenz, J. Lenzi, J. Cmaidalka, R. L. Meng, Y. Y. Sun, Y. Y. Xue, and C. W. Chu, Physica C **383**, 191 (2002).
- <sup>12</sup> N. May, W. Müller and H. Schäfer, Z. Naturforsch. B **2**, 1947 (1977).
- <sup>13</sup> F. Sano, Y. Takahashi, K. Takase, Y. Takano and K. Sekizawa, CP850 Low Temperature Physics: 24<sup>th</sup> International Conference on Low Temperature Physics, 2006.
- <sup>14</sup> The chosen doping  $x = 1$  is not far from the experimental stoichiometry ( $x = 0.75$ ) and avoids cumbersome supercell approaches and problems related to Be and Si ordering.
- <sup>15</sup> M. Lüders, M. A. L. Marques, N. N. Lathiotakis, A. Floris, G. Profeta, L. Fast, A. Continenza, S. Massidda and E. K. U. Gross, Phys. Rev. B, **72**, 024545 (2005).
- <sup>16</sup> M. A. L. Marques, M. Lüders, N. N. Lathiotakis, G. Profeta, A. Floris, L. Fast, A. Continenza, E. K. U. Gross and S. Massidda, Phys. Rev. B, **72**, 024546 (2005).
- <sup>17</sup> SELF code, (<http://www.fisica.uniroma2.it/~self/>)
- <sup>18</sup> Plane-Wave Self-Consistent-Field (PWSCF) code (<http://www.pwscf.org/>).
- <sup>19</sup> N. Troullier and J. L. Martins, Phys. Rev. B **43**, 1993 (1991).
- <sup>20</sup> M. Fuchs and M. Scheffler, Comput. Phys. Commun. **119**, 67 (1999).
- <sup>21</sup> <http://www.fhi-berlin.mpg.de/th/fhi98md/fhi98PP/>
- <sup>21</sup> J. Perdew, K. Burke, and M. Ernzerhof, Phys. Rev. Lett. **77**, 3865 (1996).
- <sup>22</sup> EXCITING code, <http://exciting.sourceforge.net/>
- <sup>23</sup> S. Baroni, S. de Gironcoli, A. Dal Corso, P. Giannozzi, Rev. Mod. Phys. **73**, 515 (2001).
- <sup>24</sup> M. Giantomassi, L. Boeri, and G. B. Bachelet, PRB **72**, 224512 (2005).
- <sup>25</sup> K. P. Bohnen, R. Heid, B. Renker, Phys. Rev. Lett. **86**, 5771 (2001).
- <sup>26</sup> A. Shukla, M. Calandra, M. d'Astuto, M. Lazzeri, F. Mauri, C. Bellin, M. Krisch, J. Karpinski, S. M. Kazakov, J. Jun, D. Daghero, and K. Parlinski Phys. Rev. Lett. **90**, 095506 (2003).
- <sup>27</sup> G. Profeta, C. Franchini, N. N. Lathiotakis, A. Floris, M. A. L. Marques, M. Lüders, S. Massidda, E. K. U. Gross, and A. Continenza, Phys. Rev. Lett. **96**, 047003 (2006).
- <sup>28</sup> A. Sanna, C. Franchini, A. Floris, G. Profeta, N. N. Lathiotakis, M. Lüders, M. A. L. Marques, E. K. U. Gross, A. Continenza, and S. Massidda Phys. Rev. B **73**, 144512 (2006).
- <sup>29</sup> A. Floris, A. Sanna, S. Massidda and E. K. U. Gross, Phys. Rev. B **75**, 054508 (2007).
- <sup>30</sup> A. Floris, A. Sanna, G. Profeta, N. N. Lathiotakis, M. Lüders, M. A. L. Marques, C. Franchini, E. K. U. Gross, A. Continenza, and S. Massidda, Physica C **456**, 45 (2007).
- <sup>31</sup> In MgB<sub>2</sub> for example, the strong hole-doped covalent B-B bond ensures an high el-ph coupling: however, an equally high repulsive Coulomb interaction reduces the superconducting critical temperature.
- <sup>32</sup> A. Brinkman, A. A. Golubov, H. Rogalla, O. V. Dolgov, J. Kortus, Y. Kong, O. Jepsen, and O. K. Andersen, Phys. Rev. B **65**, 180517 (2002).
- <sup>33</sup> A. A. Golubov, A. Brinkman, O. V. Dolgov, J. Kortus, and O. Jepsen, Phys. Rev. B **66**, 054524 (2002).
- <sup>34</sup> O. V. Dolgov, R. S. Gonnelli, G. A. Umharino, A. A. Golubov, S. V. Shulga, and J. Kortus, Phys. Rev. B **68**, 132503 (2003).
- <sup>35</sup> E. Macocian, Modern Physics Letters B, **19**, 503 (2005).
- <sup>36</sup> H. J. Choi, D. Roundy, H. Sun, M. L. Cohen, S. G. Louie, Phys. Rev. B **66**, 020513 (2002).
- <sup>37</sup> A. Floris, G. Profeta, N. N. Lathiotakis, M. Lüders, M. A. L. Marques, C. Franchini, E. K. U. Gross, A. Continenza and S. Massidda, Phys. Rev. Lett. **94**, 037004 (2005).